

Protein Structural Dynamics Revealed by Time-Resolved X-ray Solution Scattering

Jong Goo Kim,^{†,‡,⊥} Tae Wu Kim,^{†,‡,⊥} Jeongho Kim,[§] and Hyotcherl Ihée*,^{†,‡}

[†]Department of Chemistry, KAIST, Daejeon 305-701, Republic of Korea

[‡]Center for Nanomaterials and Chemical Reactions, Institute for Basic Science (IBS), Daejeon 305-701, Republic of Korea

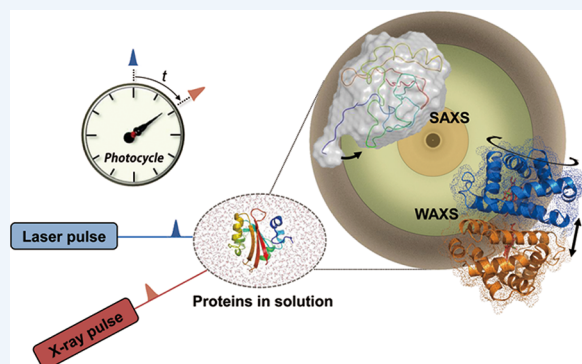
[§]Department of Chemistry, Inha University, Incheon 402-751, Republic of Korea

CONSPECTUS: One of the most important questions in biological science is how a protein functions. When a protein performs its function, it undergoes regulated structural transitions. In this regard, to better understand the underlying principle of a protein function, it is desirable to monitor the dynamic evolution of the protein structure in real time. To probe fast and subtle motions of a protein in physiological conditions demands an experimental tool that is not only equipped with superb spatiotemporal resolution but also applicable to samples in solution phase.

Time-resolved X-ray solution scattering (TRXSS), discussed in this Account, fits all of those requirements needed for probing the movements of proteins in aqueous solution. The technique utilizes a pump–probe scheme employing an optical pump pulse to initiate photoreactions of proteins and an X-ray probe pulse to monitor ensuing structural changes. The technical advances in ultrafast lasers and X-ray sources allow us to achieve superb temporal resolution down to femtoseconds. Because X-rays scatter off all atomic pairs in a protein, an X-ray scattering pattern provides information on the global structure of the protein with subangstrom spatial resolution. Importantly, TRXSS is readily applicable to aqueous solution samples of proteins with the aid of theoretical models and therefore is well suited for investigating structural dynamics of protein transitions in physiological conditions.

In this Account, we demonstrate that TRXSS can be used to probe real-time structural dynamics of proteins in solution ranging from subtle helix movement to global conformational change. Specifically, we discuss the photoreactions of photoactive yellow protein (PYP) and homodimeric hemoglobin (HbI). For PYP, we revealed the kinetics of structural transitions among four transient intermediates comprising a photocycle and, by applying structural analysis based on ab initio shape reconstruction, showed that the signaling of PYP involves the protrusion of the N-terminus with significant increase of the overall protein size. For HbI, we elucidated the dynamics of complex allosteric transitions among transient intermediates. In particular, by applying structural refinement analysis based on rigid-body modeling, we found that the allosteric transition of HbI accompanies the rotation of quaternary structure and the contraction between two heme domains.

By making use of the experimental and analysis methods presented in this Account, we envision that the TRXSS can be used to probe the structural dynamics of various proteins, allowing us to decipher the working mechanisms of their functions. Furthermore, when combined with femtosecond X-ray pulses generated from X-ray free electron lasers, TRXSS will gain access to ultrafast protein dynamics on sub-picosecond time scales.



INTRODUCTION

Proteins are complex macromolecules that play many important roles in regulating life-sustaining processes in living organisms. A protein has its specific function governed by the sequence of constituent amino acids and a resultant three-dimensional (3D) structure. A functioning protein undergoes structural changes leading to a specific functional conformation in a precisely controlled manner and can transiently reside in relatively stable intermediate conformations. Therefore, we can approximate the structural transitions of a protein by a series of quasi-equilibrium processes through those transient intermediates. In general, a transition between the transient intermediates occurs on a wide range of time scales from sub-picosecond to seconds and in

length scales from subangstroms to tens of angstroms. To probe such fast and small-amplitude motions of proteins, we need an experimental tool that is not only equipped with superb spatiotemporal resolution but also applicable to proteins in physiological conditions (that is, in aqueous solution phase).

The dynamics of protein structural transitions have been thus far studied mainly by using time-resolved spectroscopies,^{1–4} time-resolved X-ray crystallography,^{5–8} and multidimensional nuclear magnetic resonance (NMR) spectroscopy.^{9,10} However, each of those experimental methods has its own limitation, and

Received: April 11, 2015

Published: July 2, 2015

none of them satisfy all of the above requirements needed for probing rapid and small motions of proteins in solution. In this regard, time-resolved X-ray solution scattering (TRXSS), also known as time-resolved X-ray liquidography (TRXL),^{11–17} is a complementary technique well suited for investigating protein structural dynamics in solution. As schematically shown in Figure 1, the technique makes use of a pump–probe scheme employing

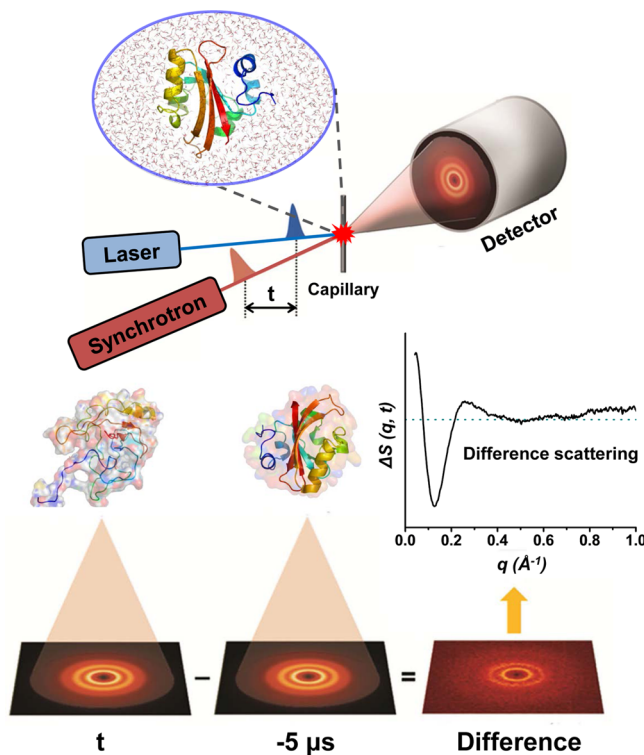


Figure 1. Schematic of TRXSS experiment. The protein in solution is excited by an optical laser (pump) pulse. After a well-defined time delay (t), an X-ray (probe) pulse generated from a synchrotron is delivered to the photoexcited sample and the scattering patterns are measured at various time delays. By taking the difference between scattering patterns measured before the laser excitation (i.e., at a negative time delay) and after the laser excitation (i.e., at a positive time delay), the transient structural change of the protein can be obtained selectively.

(1) an optical pump pulse that initiates structural transitions of photoactive proteins and (2) an X-ray probe pulse that detects ensuing structural changes after photoexcitation. Since X-rays scatter off all atomic pairs in a protein molecule, an X-ray scattering pattern provides information on the global structure of the protein with subangstrom structural sensitivity. In addition, TRXSS is readily applicable to proteins in aqueous solution with the aid of theoretical models and thus is appropriate for investigating structural dynamics of proteins in physiological conditions. Thus, TRXSS can serve as a unique and effective tool that probes the real-time structural dynamics of proteins in solution and complements other probes of protein dynamics.

■ STRUCTURAL SENSITIVITY OF TIME-RESOLVED X-RAY SOLUTION SCATTERING

TRXSS is based on elastic scattering of X-ray photons off atomic pairs in molecules and its spatial resolution is determined by the profile of scattering intensity as a function of scattering angle. Here we examine whether the spatial sensitivity of X-ray solution scattering is high enough to detect the conformational changes

involved in functional transitions of a protein. To do so, we performed molecular dynamics (MD) simulations for cytochrome c (Cyt c) and myoglobin (Mb) to highlight structural changes of large and small amplitudes, respectively. For Cyt c, we simulated the unfolding process that occurs by transitions through various conformations of different sizes. The maximum root-mean-square deviation in the positions of C_{α} atoms (C_{α} -RMSD) between the simulated unfolded structure and the native structure was 10.2 Å. For various unfolded conformations generated by the MD simulation as shown in Figure 2a, we calculated theoretical static scattering curves using Crysolv¹⁸ and subsequently obtained difference scattering curves of the unfolded conformations by subtracting the static scattering curve of the native folded structure. The difference scattering curves exhibit oscillatory features in a q -range from 0 to 0.3 Å⁻¹. The scattering intensity in this small-angle region called small-angle X-ray solution scattering (SAXS) is sensitive to the change in the overall shape and size of a protein. Accordingly, Figure 2a clearly shows that the amplitude of the difference scattering curve in the SAXS region increases gradually as the conformation of Cyt c changes toward the unfolded state, indicating that the change in the global conformation of a protein can be readily detected by TRXSS.

For Mb, we sampled various conformations using the MD simulation. Compared with the case of Cyt c, the structural variation of Mb was restrained to a much smaller degree, and two representative conformations shown in Figure 2b have C_{α} -RMSD of only 0.4 Å. As can be seen in Figure 2b, the difference scattering curves for the two representative conformations show oscillatory features in a q -range from 0.2 to 1.0 Å⁻¹. The scattering intensity in this large-angle region called wide-angle X-ray solution scattering (WAXS) is sensitive to small-amplitude motions of a protein. Accordingly, the shapes of the difference scattering curves change significantly with the change in the conformation of Mb, specifically subtle rearrangement of helices constituting the protein. This result shows that even a small variation of the protein conformation can be detected sensitively by the amplitude change of the difference scattering curve in the WAXS region and thus demonstrates that TRXSS has a potential to detect both large and small structural changes of a protein. Here we note that TRXSS is sensitive to the changes in global conformation of proteins, for example, tertiary and quaternary structural changes, and therefore its subangstrom structural sensitivity applies only to the movements of secondary structures (for example, α -helix). In contrast, time-resolved X-ray crystallography can detect atomic-level structural changes, that is, the movements of individual atoms. In this regard, TRXSS has limited spatial resolution compared with time-resolved X-ray crystallography.

■ ANALYSIS SCHEME OF TIME-RESOLVED SCATTERING DATA

Although the simulations in the previous section demonstrate that structural changes in a protein can be readily detected by the difference scattering curves, it is still challenging to extract the detailed structural changes of the protein from the scattering curves. The first step toward identifying the 3D structures of the protein intermediates is to extract the difference scattering curves that directly reflect the structural features of reaction intermediates and the transition kinetics among them. This task can be accomplished by the kinetic analysis based on singular value decomposition (SVD) and principal component analysis (PCA), which allows us to elucidate the structural dynamics of

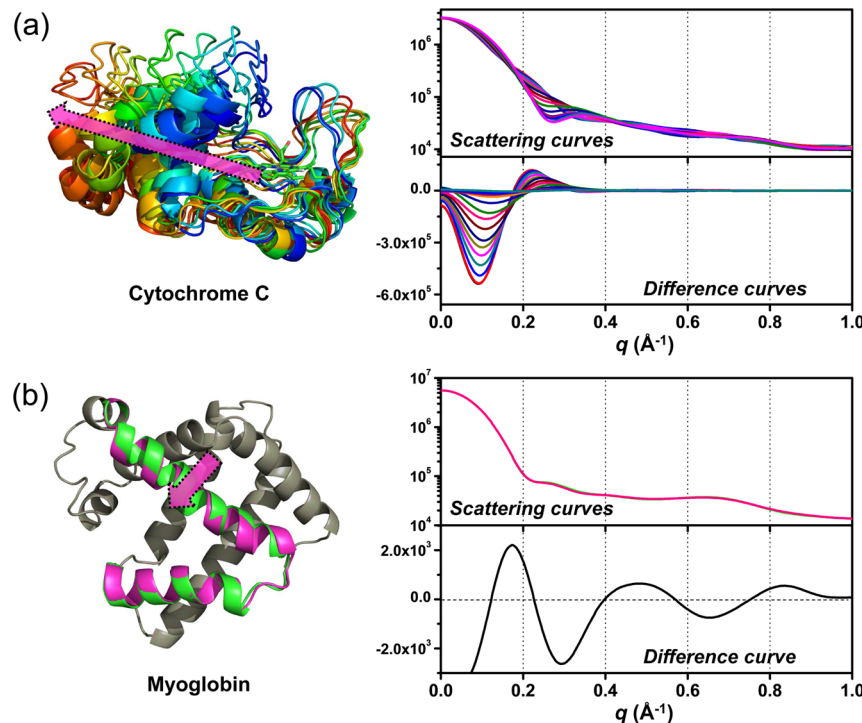


Figure 2. (a) (left) Unfolding process of Cyt c produced by MD simulation. (right) For various unfolded conformations of the protein sampled from MD snapshots, theoretical static (upper panel) and difference (lower panel) scattering curves were calculated. As the protein becomes unfolded (magenta arrow), the amplitude of the difference scattering curve in the SAXS region increases gradually. (b) (left) Helix movement of Mb produced by MD simulation. (right) For two conformations of the protein with slightly different helix positions, which can result from the clamshell movement (magenta arrow), theoretical static (upper panel) and difference (lower panel) scattering curves were calculated. The small change in the static scattering curve induced by the subtle helix movement is seen distinctly in the difference scattering curve.

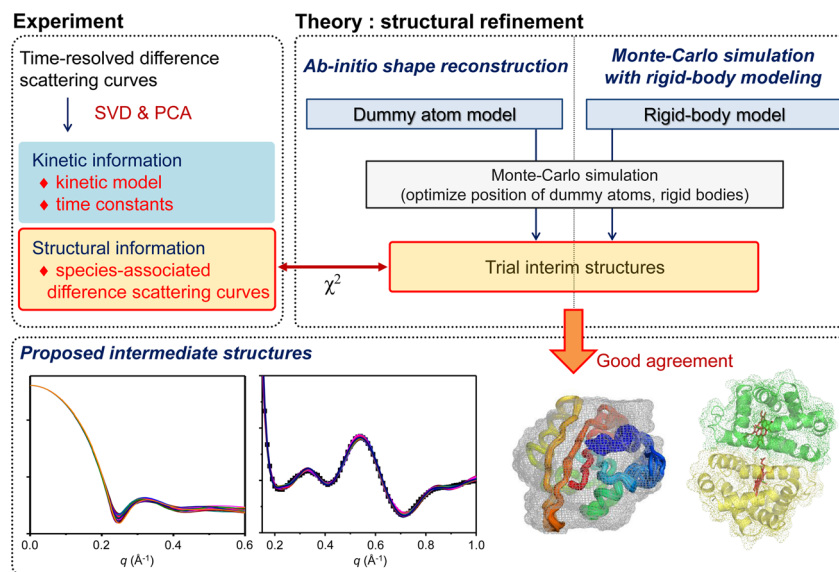


Figure 3. Overall analysis scheme of the TRXSS data. Population changes and species-associated difference scattering curves of reaction intermediates are obtained by singular value decomposition (SVD) analysis and subsequent principal component analysis (PCA). By minimizing the discrepancy (χ^2) between experimental species-associated scattering curves and theoretical scattering curves calculated from a dummy atom model or a rigid-body model, the refined structure that yields the scattering curve fitting the experimental scattering curve is determined as the structure of a protein intermediate.

proteins, including the difference scattering curves of structurally distinguishable species, so-called species-associated difference scattering curves.^{19,20} Once the species-associated difference scattering curves are obtained, they can be used to reveal the details of structural changes among the protein intermediates using structural analysis tools described below.

Ab Initio Reconstruction of Global Protein Conformation

The molecular shape of a protein intermediate can be readily extracted from the species-associated difference scattering curve by the shape reconstruction method used in conventional SAXS analysis. First, a species-associated “static” scattering curve is built for each intermediate by adding a static scattering curve for

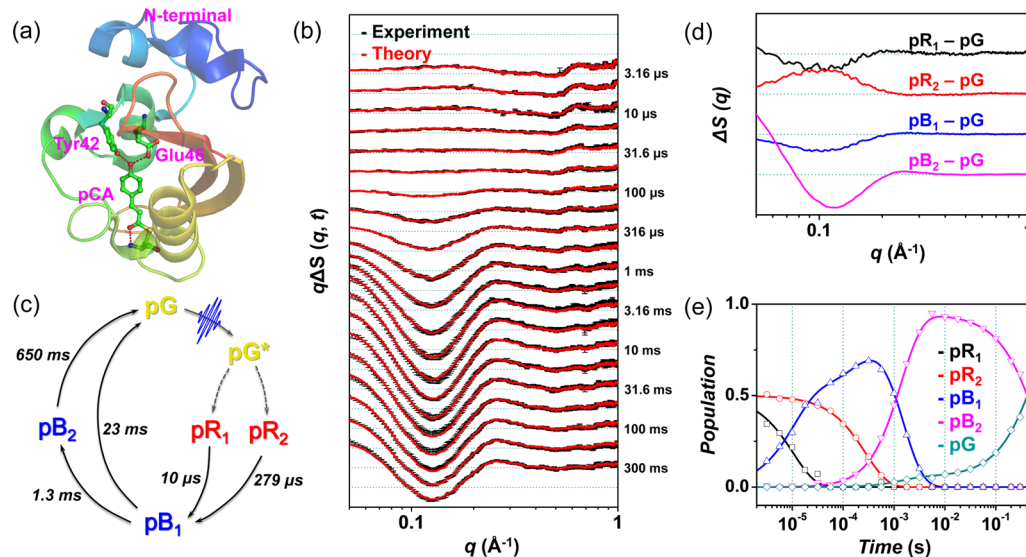


Figure 4. (a) Structure of PYP and its pCA chromophore. (b) Time-resolved difference scattering curves, $q\Delta S(q,t)$, of PYP in solution (black) and theoretical difference scattering curves (red) obtained from the kinetic analysis. (c) Proposed kinetic model of the PYP photocycle. (d) Species-associated difference scattering curves of the intermediates extracted from the kinetic analysis based on the proposed kinetic model. (e) Population changes of the individual intermediates as a function of time. The open circles correspond to the optimized populations at the time delay points where experimental data were measured, and the lines correspond to the population changes obtained by the kinetic analysis.

the ground state to the scaled species-associated difference scattering curve. Then, from the species-associated static scattering curve, a pair distribution function, $P(r)$, and the radius of gyration, R_g , are obtained for each intermediate species by the indirect Fourier transform using the GNOM software.²¹ Finally, using the optimal pair distribution function and the species-associated static scattering curve, the ab initio bead modeling is implemented to reconstruct the molecular shape of the intermediate using the DAMMIN software.²² In the ab initio shape reconstruction of a protein, the protein structure is described as a collection of densely packed bead atoms inside a constrained volume. The spatial configuration of randomly oriented bead atoms is varied until the discrepancy between the species-associated static scattering curve and the theoretical scattering curve calculated for the bead atoms is minimized. For each species-associated difference scattering curve, this reconstruction procedure is repeated multiple times to make a structure pool that reflects the structural fluctuation of the protein. From this structure pool, the representative shape of the protein is reconstructed to determine an average structure of each intermediate.

Structural Refinement Aided by Rigid-Body Modeling

Besides the molecular shape, more detailed structures of the protein intermediates can be obtained by performing structural refinement aided by rigid-body modeling applied to the difference scattering patterns in both SAXS and WAXS regions. This method is based on the assumption that the short-order structural units of the protein, for example, α -helices, in the crystal structure, which is used as the initial structure, are maintained as rigid bodies in solution. Once we divide the entire protein into several rigid bodies, we can find the optimum positions and orientations of the rigid bodies that yield a theoretical scattering curve fitting the experimental scattering curve while maintaining chemical stabilities of the protein. For the optimization, we minimize the value of a target function, E , defined by a sum of (1) a χ^2 value that represents the discrepancy between the theoretical and experimental scattering curves and

(2) a penalty value that represents chemical instability. To avoid being trapped in local energy minima, the minimization is conducted for various initial structures generated by randomly moving rigid bodies in a template crystallographic structure. The lowest target function value is searched based on a Monte Carlo simulation algorithm, which moves rigid bodies randomly. By the minimization for various initial structures, we select the protein structures that give target function values below a certain threshold as candidate structures of a protein intermediate.

The overall scheme of the data analysis for the TRXSS data of proteins is summarized in Figure 3. In following sections, we present two representative examples where the structural dynamics of photoinduced protein structural transitions were revealed using the analysis methods described above.

■ GLOBAL CONFORMATIONAL CHANGES: SIGNALING OF PHOTOACTIVE YELLOW PROTEIN

As an example of demonstrating the suitability of TRXSS to probe the global conformational changes of proteins, we investigated the photoreaction of photoactive yellow protein (PYP). PYP is a blue-light photoreceptor and serves as a signal transduction module that converts external light stimuli into a biological signal (Figure 4a).²³ On absorption of blue light, PYP undergoes a signaling process that accompanies not only the trans-to-cis isomerization of the chromophore, *p*-coumaric acid (pCA), but also the change in the global conformation of the protein matrix.^{6,24–26} Thus, PYP is a good system for demonstrating the structural sensitivity of TRXSS for global structural changes. By performing kinetic analysis on the TRXSS signals of wild-type PYP shown in Figure 4b,¹⁹ we extracted the kinetics of the PYP photocycle (Figure 4c). Specifically, the kinetic analysis yielded five kinetic components (10 μ s, 279 μ s, 1.3 ms, 23 ms, and 650 ms) associated with the structural transitions among four intermediates (termed pR₁, pR₂, pB₁, and pB₂) constituting the photocycle of PYP. From the kinetic analysis, we extracted the species-associated difference scattering curves (Figure 4d), which contain the information on the

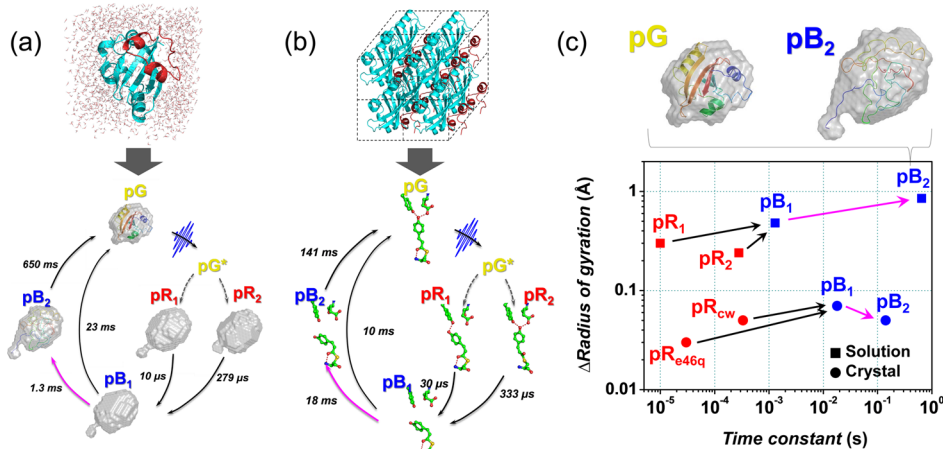


Figure 5. (a) Global molecular shapes of the protein intermediates in solution obtained by the ab initio shape reconstruction. (b) The structural change of the pCA chromophore determined from time-resolved X-ray crystallography.⁶ We note that the pR_1 and pR_2 intermediates in solution were termed as pR_{E46Q} and pR_{CW} intermediates in crystal in a previous study.^{5,6} (c) Change in the radius of gyration (R_g) for each intermediate relative to the ground-state PYP as the photocycle in solution (■) and crystal (●) progresses over time. The magenta lines emphasize the formation of a putative signaling state (pB_2) in solution and crystal. For clarity, the protein shape of pB_2 is compared with that of ground state (pG). The reconstructed shape of pB_2 state is superimposed onto the protein structure (rainbow cartoon) determined from a combination of various probes (DEER, NMR, and SAXS/WAXS).²⁷

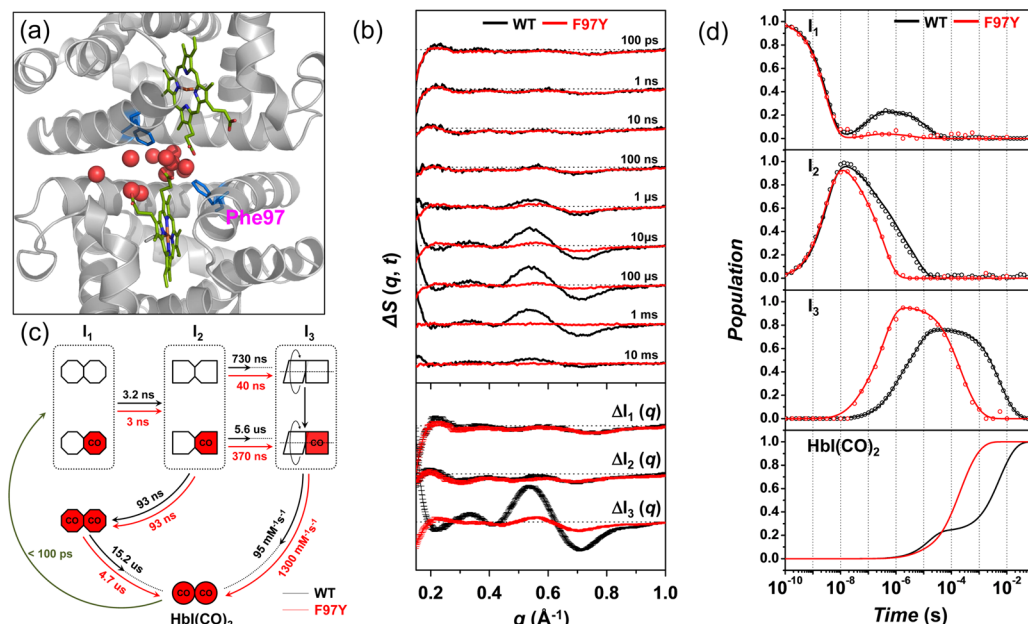


Figure 6. (a) Structure of HbI(CO)₂ (pdb code 3SDH). The Phe97 residue (shown in blue) in each subunit is replaced by tyrosine in the F97Y mutant. Two hemes (shown in green) are in contact with each other through a hydrogen-bonding network connected by well-organized interfacial water molecules (shown in red). (b) (top) Time-resolved difference scattering curves, $\Delta S(q,t)$, measured for solution samples of wild-type (black curves) and F97Y HbI (red curves). (bottom) Species-associated difference scattering curves for the three intermediates of wild-type HbI (black) and its F97Y mutant (red). (c) Kinetic model common for both wild-type and F97Y HbI. The time constants in black and red correspond to the wild-type and the mutant HbI, respectively. The red (with “CO”) and white symbols represent the ligated and photolyzed subunits, respectively. (d) Population changes of the three intermediates and HbI(CO)₂ as a function of time for the wild-type (black) and the mutant (red) HbI. The open circles and the lines have the same meaning as in Figure 3e.

structures of the transient intermediates, and time-dependent populations of individual intermediates (Figure 4e). The species-associated difference scattering curves in Figure 4d show significant amplitudes in the small-angle region from 0.04 to 0.3 Å⁻¹, indicating the change in global conformation of the entire protein.

Extracting the Global Conformational Changes

While we can have a rough estimate of the structural change of a protein from the oscillatory pattern of a difference scattering

curve, a more intuitive picture can be obtained by characterizing the shape of a protein molecule in real space. To do so, we performed structural analysis based on the ab initio shape reconstruction as described in a previous section. According to the result of the shape reconstruction shown in Figure 5a, one side of the protein protrudes in the transitions to the pR_1 and pR_2 intermediates, and the protrusion grows up gradually with the progress of the photocycle, resulting in the pB_2 intermediate with the maximum protein volume estimated from the radius of gyration (R_g). In particular, the molecular shape of pB_2 is in good

agreement with the atomistic structure of a putative signaling state of wild-type PYP (PDB code 2KX6) determined from a combination of multiple structural probes (DEER, NMR, and X-ray scattering).²⁷ This good agreement confirms the integrity of the protein conformation reconstructed from the TRXSS data alone. The protruded part observed in all the intermediates of the PYP photocycle was assigned to the N-terminal region.

Comparison of Kinetics and Structural Dynamics in the Solution and Crystalline Phases

The kinetics extracted from the TRXSS data provides a rare opportunity to directly compare the effect of environment on the protein kinetics. It turned out that, as shown in Figure 5a,b, the kinetic model for the photocycle of PYP in solution phase determined by TRXSS is consistent with the one in crystalline phase obtained by time-resolved Laue X-ray crystallography.⁶ Specifically, the photoexcited PYP in both crystalline and solution phases undergoes bifurcated transitions through two types of red-shifted intermediates (pR_1 and pR_2) to the blue-shifted pB_1 intermediate on comparable time scales. On the other hand, the $pB_1 \rightarrow pB_2$ transition, which leads to the formation of the signaling state, exhibits very different dynamics in the two phases, that is, the $pB_1 \rightarrow pB_2$ transition occurs in 1.3 ms in solution but is much slower in crystal (18 ms). By contrast, the recovery of pG from pB_2 is accelerated in the crystalline phase. To compare the extent of the conformational changes with the progress of the PYP photocycle in crystal and solution, we plotted in Figure 5c the change of R_g for each intermediate relative to the pG structure. It can be seen that the change of R_g in solution (0.9 Å) is 1 order of magnitude larger than that in the crystal (0.07 Å). The movement of the N-terminal region is restricted in the crystal due to crystal contact whereas the N-terminus can move freely in solution. The slow $pB_1 \rightarrow pB_2$ transition accompanying small conformational change and the accelerated recovery of pG in the crystalline phase directly demonstrate how the crystal contacts affect the structural dynamics of PYP.

SUBTLE STRUCTURAL TRANSITIONS: ALLOSTERIC TRANSITION OF HOMODIMERIC HEMOGLOBIN

As shown above, PYP involves rather large conformational changes, but many proteins effect only small structural perturbations. For example, crystal structures of the oxygenated (relaxed, R) and deoxygenated (tense, T) states of homodimeric hemoglobin (HbI) characterized by X-ray crystallography^{28,29} exhibit a small structural difference, giving only 0.6 Å RMSD. HbI has a simpler structure than hemoglobin (Figure 6a) and exhibits cooperative ligand binding activity, and therefore it is a good model system for studying allosteric structural changes. However, detailed structural dynamics of HbI associated with the allosteric effect had not been understood completely. To address these questions and examine the effect of the mutation on the protein structural transition, we applied TRXSS to the wild-type HbI protein ligated with CO ligands, HbI(CO)₂, and its F97Y mutant, where Phe97 in each subunit was replaced by tyrosine. It has been known that the Phe97 residue is flipped during the R-T transition.²⁸

Kinetics of HbI and the Effect of Mutation

TRXSS signals of wild-type and F97Y HbI are very different from each other after 1 μs as can be seen in Figure 6b, showing the effect of mutation on the structural dynamics of the allosteric transition. By performing kinetic analysis based on SVD and PCA on the TRXSS signals, we extracted the kinetics of the allosteric

transition. We identified three structurally distinct intermediates termed I_1 , I_2 , and I_3 that undergo structural transitions following a kinetic model common for both wild-type and F97Y (Figure 6c).²⁰ The kinetics show that the transition from I_2 to I_3 has two time constants depending on the degree of the ligand dissociation and thus reveal that the singly liganded and unliganded forms of each intermediate share the same structure, providing direct evidence that the ligand photolysis of only a single subunit induces the same structural change as the complete photolysis of both subunits does. In addition, the overall kinetics is accelerated by an order of magnitude in F97Y, except for the I_1 -to- I_2 transition and the I_2 -to- I_1 geminate recombination. Especially, in F97Y, the R-T transition from I_2 to I_3 is accelerated significantly and becomes faster than the geminate recombination, resulting in practical quenching of the geminate recombination (Figure 6d). The acceleration in F97Y is consistent with a stronger ligand binding affinity of the mutant. The wild-type and F97Y forms have identical species-associated difference scattering curves for the I_1 and I_2 intermediates (Figure 6b), indicating the negligible effect of the mutation on the structures of I_1 and I_2 . In contrast, the wild-type and the F97Y mutant forms show distinctively different species-associated difference scattering curves for the I_3 intermediate, meaning that the structure of the I_3 intermediate is greatly perturbed by the F97Y mutation. To distinguish the two different structures of the I_3 intermediate, we labeled them as I_3^{WT} and I_3^{F97Y} for the wild-type and the F97Y mutant forms, respectively.

Structural Dynamics of HbI

The detailed structures of the intermediates involved in the allosteric transition of HbI can be extracted by performing structural refinement aided by rigid-body modeling on the species-associated difference scattering curves of I_1 , I_2 , I_3^{WT} , and I_3^{F97Y} as described in a previous section.²⁰ From the structural refinement, for each intermediate, we obtained a number of candidate structures whose theoretical scattering curves well match the corresponding experimental species-associated difference scattering curve as shown in Figure 7a.

The details of tertiary structural changes of wild-type HbI can be visualized by displacement plots, which show the displacements of amino acid residues induced by a protein structural transition as a function of the amino acid sequence. The displacement is defined by the difference in distance between the C_α atom in a residue and the iron atom of the heme in the same subunit. The displacement plots of the candidate structures of individual intermediates are shown in Figure 7b (upper panel), where the displacements of I_1 , I_2 and I_3^{WT} were calculated relative to HbI(CO)₂, I_1 , and I_2 , respectively. The average displacement plot of I_1 relative to HbI(CO)₂ shows that the CD loop (residue 50–59) and the G helix move away from the heme while the E and F helices move toward the heme in the transition from HbI(CO)₂ to I_1 . The displacement plot of I_2 relative to I_1 exhibits only slight fluctuation, indicating that the tertiary structure remains nearly intact during the transition from I_1 to I_2 . Then, the transition from I_2 to I_3^{WT} accompanies the rearrangement of all the helices as shown in the displacement plot of I_3^{WT} relative to I_2 . The displacement plots of I_3^{WT} and the crystallographic structure of deoxy HbI (PDB code 4SDH) relative to the structure of HbI(CO)₂ (PDB code 3SDH) are similar to each other, except for terminal regions, as shown in Figure 7b (lower panel). This observation indicates that the tertiary structure of I_3^{WT} in solution is similar to the structure of the T-state in crystal. The smaller displacements of the helices in the terminal regions of HbI in the

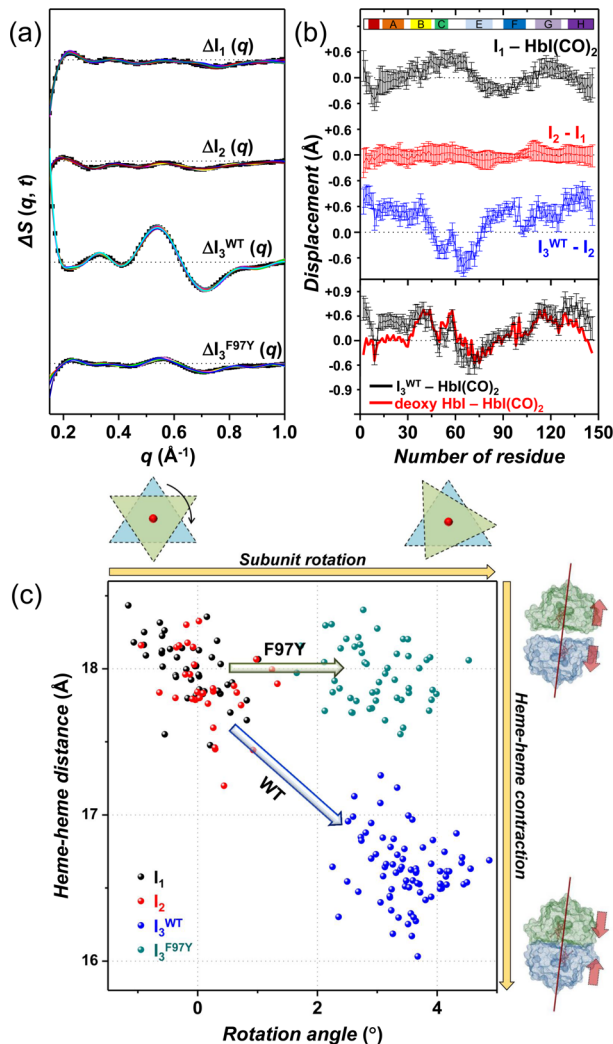


Figure 7. (a) Experimental species-associated difference scattering curves (squares) and theoretical difference scattering curves (solid lines) for the four intermediates. (b) (top) Averaged displacement plots of the three intermediates of wild-type HbI (solid lines). Error bars represent standard deviation values among various candidate structures of each intermediate. (bottom) Displacement plots of I₃^{WT} (black) and the crystallographic structure of deoxy-HbI (red) relative to HbI(CO)₂. (c) Heme–heme distances in the candidate structures of the four intermediates represented as a function of subunit rotation angle. Dots in black, red, blue, and green correspond to I₁, I₂, I₃^{WT}, and I₃^{F97Y}, respectively. The blue arrow indicates that the transition from I₂ to I₃^{WT} involves the rotation of subunits and the decrease of the heme–heme distance, while the green one indicates that the transition from I₂ to I₃^{F97Y} does not accompany any decrease of the heme–heme distance.

crystalline phase can be attributed to the restricted movements by crystal contacts.

Subunit Rotation and Contraction of HbI

We also quantified the quaternary structural changes using a couple of structural parameters, the angle of subunit rotation and the distance between the iron atoms of hemes. Those two structural parameters are key parameters that describe quaternary structural change because the ligand-binding affinity of HbI is modulated by the subunit rotation and the hydrogen-bonding network connecting the two hemes.^{30,31} Figure 7c shows the subunit rotation angles and the heme–heme distances

in the candidate structures of individual intermediates. The formation of I₁ and I₂ does not involve any notable subunit rotation or contraction of the heme–heme distance. By contrast, the transition from I₂ to I₃^{WT} accompanies the rotation of subunits (subunit rotation angle = 3.4°) and the decrease of the heme–heme distance (by 1.3 Å). Based on this result, we concluded that I₁ and I₂ correspond to the R states and I₃^{WT} is equivalent to the T state. For F97Y HbI, we can see that the formation of I₃^{F97Y} accompanies the subunit rotation by 2.9° but does not involve any decrease of the heme–heme distance. The unchanged heme–heme distance of I₃^{F97Y} can be explained by considering the presence of Tyr97 facing the interface in a deoxy form.²⁸

CONCLUSION AND FUTURE OUTLOOK

In this Account, we demonstrated that TRXSS has structural sensitivity enough to probe the large- and small-amplitude motions of proteins in real time, for example, the change in the global conformation and even subtle tertiary and quaternary structural changes. Although TRXSS has been thus far very successful in revealing the structural dynamics of proteins in solution, there still remains much room for further improvement. For example, by combining TRXSS with MD simulations,³² we may obtain rather direct information on the transition kinetics and pathways at the atomic level. Also, considering that the structural information contained in time-resolved solution scattering data is limited compared with that of crystallographic data, a variety of schemes to increase the information content are under development, such as anisotropic scattering³³ and heavy-atom labeling. In addition, with the development of X-ray free electron lasers (XFELs), the time resolution of TRXSS^{34,35} and time-resolved X-ray crystallography³⁶ has been improved down to femtosecond time scale. By performing femtosecond X-ray solution scattering at XFEL facilities, one will be able to make a leap forward to investigate ultrafast dynamics of proteins on sub-picosecond time scales.

AUTHOR INFORMATION

Corresponding Author

*E-mail: hyotcherl.ihee@kaist.ac.kr.

Author Contributions

†J.G.K. and T.W.K. contributed equally.

Notes

The authors declare no competing financial interest.

Biographies

Jong Goo Kim is a Ph.D. student in the Department of Chemistry at KAIST. His present research is aimed at investigating ultrafast structural dynamics of various molecules using time-resolved X-ray solution scattering.

Tae Wu Kim is a Ph.D. student in the Department of Chemistry at KAIST. His present research focuses on investigating ultrafast dynamics of photoactive molecules using time-resolved X-ray solution scattering and ultrafast optical spectroscopy.

Jeongho Kim is an assistant professor in the Department of Chemistry at Inha University. He obtained his B.Sc. degree in chemistry from KAIST and his Ph.D. degree in chemistry from the University of Chicago in 2004. Then, he undertook postdoctoral studies at the University of Toronto and at KAIST. His present research focuses on investigating fast dynamics occurring in electronic excited states of molecular systems and nanoscale materials using time-resolved optical spectroscopy and TRXSS.

Hyotcherl Ihée is a professor in the Department of Chemistry at KAIST. His current research interests focus on probing molecular structural dynamics using time-resolved X-ray/electron diffraction and time-resolved spectroscopy.

ACKNOWLEDGMENTS

The authors appreciate many colleagues who contributed to this work over the years. This work was supported by IBS-R004-G2, by the Basic Science Research Program through the National Research Foundation of Korea (NRF) funded by the Ministry of Science, ICT & Future Planning (NRF-2014R1A1A1002511), and by the TJ Park Science Fellowship of POSCO TJ Park Foundation.

REFERENCES

- (1) Kukura, P.; McCamant, D. W.; Mathies, R. A. Femtosecond stimulated Raman spectroscopy. *Annu. Rev. Phys. Chem.* **2007**, *58*, 461–488.
- (2) Kennis, J. T. M.; Larsen, D. S.; Ohta, K.; Facciotti, M. T.; Glaeser, R. M.; Fleming, G. R. Ultrafast protein dynamics of bacteriorhodopsin probed by photon echo and transient absorption spectroscopy. *J. Phys. Chem. B* **2002**, *106*, 6067–6080.
- (3) Zanni, M. T.; Hochstrasser, R. M. Two-dimensional infrared spectroscopy: a promising new method for the time resolution of structures. *Curr. Opin. Struct. Biol.* **2001**, *11*, 516–522.
- (4) Lewis, J. W.; Goldbeck, R. A.; Kliger, D. S.; Xie, X. L.; Dunn, R. C.; Simon, J. D. Time-resolved circular-dichroism spectroscopy - experiment, theory, and applications to biological-systems. *J. Phys. Chem.* **1992**, *96*, 5243–5254.
- (5) Jung, Y. O.; Lee, J. H.; Kim, J.; Schmidt, M.; Moffat, K.; Srajer, V.; Ihée, H. Volume-conserving trans-cis isomerization pathways in photoactive yellow protein visualized by picosecond X-ray crystallography. *Nat. Chem.* **2013**, *5*, 212–220.
- (6) Ihée, H.; Rajagopal, S.; Srajer, V.; Pahl, R.; Anderson, S.; Schmidt, M.; Schotte, F.; Anfinrud, P. A.; Wulff, M.; Moffat, K. Visualizing reaction pathways in photoactive yellow protein from nanoseconds to seconds. *Proc. Natl. Acad. Sci. U. S. A.* **2005**, *102*, 7145–7150.
- (7) Schmidt, M.; Srajer, V.; Henning, R.; Ihée, H.; Purwar, N.; Tenboer, J.; Tripathi, S. Protein energy landscapes determined by five-dimensional crystallography. *Acta Crystallogr., Sect. D: Biol. Crystallogr.* **2013**, *69*, 2534–2542.
- (8) Lorenc, M.; Hebert, J.; Moisan, N.; Trzop, E.; Servol, M.; Buron-Le Cointe, M.; Cailleau, H.; Boillot, M. L.; Pontecorvo, E.; Wulff, M.; Kosihara, S.; Collet, E. Successive dynamical steps of photoinduced switching of a molecular Fe(III) spin-crossover material by time-resolved X-Ray diffraction. *Phys. Rev. Lett.* **2009**, *103*, 028301.
- (9) Bax, A. Two-dimensional NMR and protein-structure. *Annu. Rev. Biochem.* **1989**, *58*, 223–256.
- (10) Schanda, P.; Forge, V.; Brutscher, B. Protein folding and unfolding studied at atomic resolution by fast two-dimensional NMR spectroscopy. *Proc. Natl. Acad. Sci. U. S. A.* **2007**, *104*, 11257–11262.
- (11) Malmerberg, E.; Omran, Z.; Hub, J. S.; Li, X. W.; Katona, G.; Westenhoff, S.; Johansson, L. C.; Andersson, M.; Cammarata, M.; Wulff, M.; van der Spoel, D.; Davidsson, J.; Specht, A.; Neutze, R. Time-resolved WAXS reveals accelerated conformational changes in iodoretinal-substituted proteorhodopsin. *Biophys. J.* **2011**, *101*, 1345–1353.
- (12) Ihée, H. Visualizing solution-phase reaction dynamics with time-resolved X-ray liquidography. *Acc. Chem. Res.* **2009**, *42*, 356–366.
- (13) Christensen, M.; Haldrup, K.; Bechgaard, K.; Feidenhans'l, R.; Kong, Q. Y.; Cammarata, M.; Lo Russo, M.; Wulff, M.; Harrit, N.; Nielsen, M. M. Time-resolved X-ray scattering of an electronically excited state in solution. structure of the (3)A(2u) state of tetrakis-mu-pyrophosphotodiplatinate(II). *J. Am. Chem. Soc.* **2009**, *131*, 502–508.
- (14) Cammarata, M.; Levantino, M.; Schotte, F.; Anfinrud, P. A.; Ewald, F.; Choi, J.; Cupane, A.; Wulff, M.; Ihée, H. Tracking the structural dynamics of proteins in solution using time-resolved wide-angle X-ray scattering. *Nat. Methods* **2008**, *5*, 881–886.
- (15) Ihée, H.; Lorenc, M.; Kim, T. K.; Kong, Q. Y.; Cammarata, M.; Lee, J. H.; Bratos, S.; Wulff, M. Ultrafast X-ray diffraction of transient molecular structures in solution. *Science* **2005**, *309*, 1223–1227.
- (16) Plech, A.; Wulff, M.; Bratos, S.; Mirloup, F.; Vuilleumier, R.; Schotte, F.; Anfinrud, P. A. Visualizing chemical reactions in solution by picosecond X-ray diffraction. *Phys. Rev. Lett.* **2004**, *92*, 125505.
- (17) Konuma, T.; Kimura, T.; Matsumoto, S.; Goto, Y.; Fujisawa, T.; Fersht, A. R.; Takahashi, S. Time-resolved small-angle X-ray scattering study of the folding dynamics of barnase. *J. Mol. Biol.* **2011**, *405*, 1284–1294.
- (18) Svergun, D.; Barberato, C.; Koch, M. H. J. CRYSTOL - A program to evaluate X-ray solution scattering of biological macromolecules from atomic coordinates. *J. Appl. Crystallogr.* **1995**, *28*, 768–773.
- (19) Kim, T. W.; Lee, J. H.; Choi, J.; Kim, K. H.; van Wilderen, L. J.; Guerin, L.; Kim, Y.; Jung, Y. O.; Yang, C.; Kim, J.; Wulff, M.; van Thor, J. J.; Ihée, H. Protein structural dynamics of photoactive yellow protein in solution revealed by pump-probe X-ray solution scattering. *J. Am. Chem. Soc.* **2012**, *134*, 3145–3153.
- (20) Kim, K. H.; Muniappan, S.; Oang, K. Y.; Kim, J. G.; Nozawa, S.; Sato, T.; Kosihara, S. Y.; Henning, R.; Kosheleva, I.; Ki, H.; Kim, Y.; Kim, T. W.; Kim, J.; Adachi, S.; Ihée, H. Direct observation of cooperative protein structural dynamics of homodimeric hemoglobin from 100 ps to 10 ms with pump-probe X-ray solution scattering. *J. Am. Chem. Soc.* **2012**, *134*, 7001–7008.
- (21) Svergun, D. I. Determination of the regularization parameter in indirect-transform methods using perceptual criteria. *J. Appl. Crystallogr.* **1992**, *25*, 495–503.
- (22) Svergun, D. I. Restoring low resolution structure of biological macromolecules from solution scattering using simulated annealing. *Biophys. J.* **1999**, *77*, 2896.
- (23) Henry, J. T.; Crosson, S. Ligand-binding PAS domains in a genomic, cellular, and structural context. *Annu. Rev. Microbiol.* **2011**, *65*, 261–286.
- (24) Xie, A. H.; Kelemen, L.; Hendriks, J.; White, B. J.; Hellingwerf, K. J.; Hoff, W. D. Formation of a new buried charge drives a large-amplitude protein quake in photoreceptor activation. *Biochemistry* **2001**, *40*, 1510–1517.
- (25) Yeremenko, S.; van Stokkum, I. H. M.; Moffat, K.; Hellingwerf, K. J. Influence of the crystalline state on photoinduced dynamics of photoactive yellow protein studied by ultraviolet-visible transient absorption spectroscopy. *Biophys. J.* **2006**, *90*, 4224–4235.
- (26) Hoshihara, Y.; Imamoto, Y.; Kataoka, M.; Tokunaga, F.; Terazima, M. Conformational changes in the N-terminal region of photoactive yellow protein: A time-resolved diffusion study. *Biophys. J.* **2008**, *94*, 2187–2193.
- (27) Ramachandran, P. L.; Lovett, J. E.; Carl, P. J.; Cammarata, M.; Lee, J. H.; Jung, Y. O.; Ihée, H.; Timmel, C. R.; van Thor, J. J. The short-lived signaling state of the photoactive yellow protein photoreceptor revealed by combined structural probes. *J. Am. Chem. Soc.* **2011**, *133*, 9395–9404.
- (28) Knapp, J. E.; Bonham, M. A.; Gibson, Q. H.; Nichols, J. C.; Royer, W. E., Jr. Residue F4 plays a key role in modulating oxygen affinity and cooperativity in Scapharca dimeric hemoglobin. *Biochemistry* **2005**, *44*, 14419–14430.
- (29) Royer, W. E. High-resolution crystallographic analysis of a cooperative dimeric hemoglobin. *J. Mol. Biol.* **1994**, *235*, 657–681.
- (30) Rousseau, D. L.; Song, S.; Friedman, J. M.; Boffi, A.; Chiancone, E. Heme-heme interactions in a homodimeric cooperative hemoglobin. Evidence from transient Raman scattering. *J. Biol. Chem.* **1993**, *268*, 5719–5723.
- (31) Knapp, J. E.; Gibson, Q. H.; Cushing, L.; Royer, W. E., Jr. Restricting the ligand-linked heme movement in Scapharca dimeric hemoglobin reveals tight coupling between distal and proximal contributions to cooperativity. *Biochemistry* **2001**, *40*, 14795–14805.
- (32) Zuo, X. B.; Cui, G. L.; Merz, K. M.; Zhang, L. G.; Lewis, F. D.; Tiede, D. M. X-ray diffraction “fingerprinting” of DNA structure in solution for quantitative evaluation of molecular dynamics simulation. *Proc. Natl. Acad. Sci. U. S. A.* **2006**, *103*, 3534–3539.

- (33) Kim, J.; Kim, K. H.; Kim, J. G.; Kim, T. W.; Kim, Y.; Ihee, H. Anisotropic picosecond X-ray solution scattering from photoselectively aligned protein molecules. *J. Phys. Chem. Lett.* **2011**, *2*, 350–356.
- (34) Kim, K. H.; Kim, J. G.; Nozawa, S.; Sato, T.; Oang, K. Y.; Kim, T. W.; Ki, H.; Jo, J.; Park, S.; Song, C.; Ogawa, K.; Togashi, T.; Tono, K.; Yabashi, M.; Ishikawa, T.; Kim, J.; Ryoo, R.; Ihee, H.; Adachi, S. Direct observation of bond formation in solution with femtosecond X-ray scattering. *Nature* **2015**, *518*, 385–389.
- (35) Arnlund, D.; Johansson, L. C.; Wickstrand, C.; Barty, A.; Williams, G. J.; Malmerberg, E.; Davidsson, J.; Milathianaki, D.; DePonte, D. P.; Shoeman, R. L.; Wang, D. J.; James, D.; Katona, G.; Westenhoff, S.; White, T. A.; Aquila, A.; Bari, S.; Berntsen, P.; Bogan, M.; van Driel, T. B.; Doak, R. B.; Kjaer, K. S.; Frank, M.; Fromme, R.; Grotjohann, I.; Henning, R.; Hunter, M. S.; Kirian, R. A.; Kosheleva, I.; Kupitz, C.; Liang, M. N.; Martin, A. V.; Nielsen, M. M.; Messerschmidt, M.; Seibert, M. M.; Sjohamn, J.; Stellato, F.; Weierstall, U.; Zatsepин, N. A.; Spence, J. C. H.; Fromme, P.; Schlichting, I.; Boutet, S.; Groenhof, G.; Chapman, H. N.; Neutze, R. Visualizing a protein quake with time-resolved X-ray scattering at a free-electron laser. *Nat. Methods* **2014**, *11*, 923–926.
- (36) Tenboer, J.; Basu, S.; Zatsepин, N.; Pande, K.; Milathianaki, D.; Frank, M.; Hunter, M.; Boutet, S.; Williams, G. J.; Koglin, J. E.; Oberthuer, D.; Heymann, M.; Kupitz, C.; Conrad, C.; Coe, J.; Roy-Chowdhury, S.; Weierstall, U.; James, D.; Wang, D. J.; Grant, T.; Barty, A.; Yefanov, O.; Scales, J.; Gati, C.; Seuring, C.; Srajer, V.; Henning, R.; Schwander, P.; Fromme, R.; Ourmazd, A.; Moffat, K.; Van Thor, J. J.; Spence, J. C. H.; Fromme, P.; Chapman, H. N.; Schmidt, M. Time-resolved serial crystallography captures high-resolution intermediates of photoactive yellow protein. *Science* **2014**, *346*, 1242–1246.